A compensated heat-pulse calorimeter for low temperatures

H. Wilhelm, T. Lühmann, T. Rus, and F. Steglich
Max Planck Institute for Chemical Physics of Solids, Nöthnitzer Strasse 40, 01187 Dresden, Germany

(Received 16 October 2003; accepted 8 April 2004; published 13 August 2004)

We describe a technique for measuring heat capacities ($C_{\min} \approx 1\ \mu$J/K at 0.1 K) of small solid samples at low temperatures ($0.03\ \mathrm{K} < T < 6\ \mathrm{K}$) and in high magnetic fields ($B < 12$ T). In this compensated heat-pulse technique the thermal losses are compensated through a background heating. A detailed analysis of the heat flow takes the heat input and losses into account. Test measurements on tin and $YbRh_2(Si_{0.95}Ge_{0.05})_2$ showed that the heat capacity can be determined with high precision in a fast and accurate way. This technique provides a versatile calorimeter for a wide range of heat capacities which achieves its main performance if several sample platforms are mounted and one sample is measured while the other may cool down. © *2004 American Institute of Physics.* [DOI: 10.1063/1.1771486]

I. INTRODUCTION

The measurement of the temperature dependence of the heat capacity of a material is an often used means to achieve a first step into the understanding of its physical properties. Besides the adiabatic technique several nonadiabatic techniques, like the relaxation-time method,[1] the continuous-warming principle[2] or the ac-calorimetry[3] are used. For more details the reader is referred to review articles covering low-temperature calorimetry.[4–7] The demand of a fast, versatile, and sensitive low-temperature calorimeter for small solid samples ($1\ \mathrm{mg} < m < 50\ \mathrm{mg}$) in magnetic fields ($B < 12$ T) has led to the realization of the compensated heat-pulse technique.

We would like to emphasize that the setup described here is based on the semiadiabatic heat-pulse method used by the Phillips group at Berkeley. A first description of the method was given in the article by Fisher and co-workers.[8] The calorimeter described in the following can be used for much lower temperatures ($T \approx 30$ mK) than that used so far.[9,10] The actual setup compensates the inevitable heat losses during the measurement with an adjustable background heating. This compensation makes a rapid data acquisition possible. It is much faster than a relaxation-time technique since the time consuming tracking and stabilization of the calorimeter temperature is not needed. This benefit is not obtained on the expense of accuracy and sensitivity: The precision of the heat capacity data is as high as those of the relaxation-time technique.

II. METHOD

The definition of the heat capacity,

$$C = \lim_{\Delta T \to 0} \frac{\Delta Q}{\Delta T}, \tag{1}$$

implies that an increase of the sample temperature by ΔT, caused by a supplied heat ΔQ, was achieved adiabatically. A low-temperature calorimeter ($T < 4$ K) must have a thermal link between sample and surrounding to cool the sample. One possibility is to install a heat switch. Mechanical or superconducting switches are often cumbersome or not suitable in high magnetic fields. In the present calorimeter the thermal conductance of the mounting threads and electrical leads for heater and thermometer was a compromise between the time necessary to cool the sample to ≈30 mK and the capability to compensate the heat losses during the measurement. The thermal conductance of the selected threads allows the heat capacity of the sample on the platform to be measured up to 6 K while the heat sink remains at the base temperature of the cryostat.

Figure 1(a) shows the heat-flow scheme of the sample/platform assembly. A weak thermal link, with thermal conductance K_1, establishes the connection between platform and the thermal bath. The model takes the thermal conductance K_2 ($K_2 \gg K_1$) between platform and sample explicitly into account. In the steady state and at a constant heat sink temperature (T_b) an appropriately chosen background heating power supplies the constant electrical power P_b into the heater. It compensates the heat loss through the thermal link and ensures a constant temperature of sample (T_S) and platform (T_P), i.e., $T_P = T_S \equiv T_0$ [see. Fig. 1(b)]. A heat pulse P_h of duration Δt_h adds the heat $\Delta Q_h = P_h \Delta t_h$ to the platform and T_P increases. After the heat-pulse power is switched off, the sample temperature relaxes towards the steady-state temperature $T_0 + \Delta T$, if the new background heating power was correctly adjusted.[11] For a measuring cycle (of duration Δt) the average heat capacity C_S of the sample (at the mean temperature $T_0 + \frac{1}{2}\Delta T$) is given by the ratio of the *effectively* deposited heat $\Delta Q = \Delta Q_h - \Delta P_b \Delta t$ to the achieved temperature increase ΔT. This qualitative description of the compensated heat-pulse technique can be set into a mathematical model. In the following it is shown that the measured heat capacity is correct up to the order of $K_1/K_2 \ll 1$.

The total power, $P_P(t)$, deposited on the platform is given by the heat-flow scheme of Fig. 1(a),

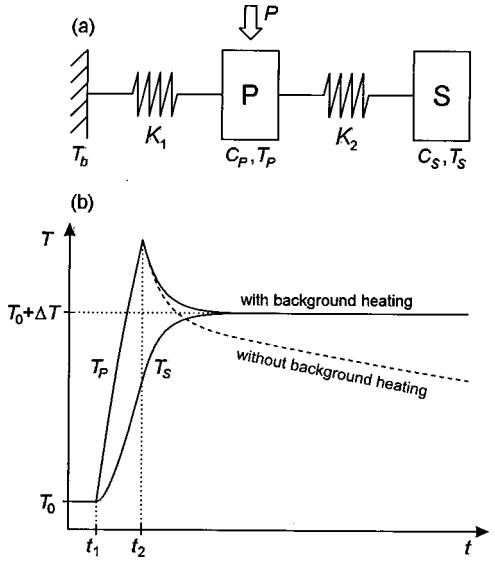

FIG. 1. (a) Heat-flow scheme of the compensated heat-pulse technique. The thermal conductances K_1 between thermal bath (T_b) and platform (P) and K_2 between sample (S) and platform are explicitly taken into account. The thermal bath remains at $T_b \leqslant 30$ mK while the supplied heating power P increases the temperature of sample (T_S) and platform (T_P) up to 6 K. C_P and C_S denote the heat capacities of platform and sample, respectively. (b) Time dependence of T_S and T_P (Ref. 11). A heat pulse during $\Delta t_h = t_2 - t_1$ delivers the heat ΔQ_h to the platform and yields a temperature increase by ΔT. An adjustable background heating compensates the heat losses through the thermal link and maintains a constant ΔT for $t > t_2$. Without additional background heating the temperature would exponentially approach T_0 (dashed line).

$$P_P(t) = P_h - K_1(T_P - T_0) - K_2(T_P - T_S). \tag{2}$$

As a consequence, the platform temperature increases from its initial value $T_P(t=t_1) = T_0 := T_{P,0}$ to

$$T_P(t) = T_{P,0} + \int_{t_1}^{t_2} \frac{P_P}{C_P} dt, \tag{3}$$

with C_P the heat capacity of the platform. Similarly, the sample temperature increases from $T_S(t=t_1) = T_0 := T_{S,0}$ to

$$T_S(t) = T_{S,0} + \int_{t_1}^{t_2} \frac{P_S}{C_S} dt, \tag{4}$$

with C_S the heat capacity of the sample and

$$P_S(t) = K_2(T_P - T_S), \tag{5}$$

the power arriving at the sample. These equations yield the time dependence of $T_P(t)$ described by

$$\frac{C_S C_P}{K_1 K_2} \ddot{T} + \left(\frac{C_S + C_P}{K_1} + \frac{C_S}{K_2} \right) \dot{T} + T = \frac{P_h}{K_1} + T_0. \tag{6}$$

The general solution for $T_P(t)$ is

$$T_P(t) = A_1 e^{-t/\tau_1} + A_2 e^{-t/\tau_2} + \frac{P_h}{K_1} + T_0. \tag{7}$$

A similar differential equation for $T_S(t)$ leads to

$$T_S(t) = B_1 e^{-t/\tau_1} + B_2 e^{-t/\tau_2} + \frac{P_h}{K_1} + T_0. \tag{8}$$

In Eqs. (7) and (8) the time constants τ_1 and τ_2 refer to the positive and negative signs, respectively, in the expression

$$\tau_{1,2} = \frac{1}{2K_1K_2}[(C_S + C_P)K_2 + C_S K_1 \pm \sqrt{[(C_S + C_P)K_2 + C_S K_1]^2 - 4C_S C_P K_1 K_2}]. \tag{9}$$

The coefficients A_1, A_2, B_1, and B_2 are given by the starting conditions at $t=0$,

$$A_{1,2} = \frac{1}{\tau_{1,2} - \tau_{2,1}} \left\{ \frac{C_S}{K_1}(T_{S,0} - T_{P,0}) + \left[\frac{C_S}{K_2} - \tau_{1,2} \right] \left[\frac{P_h}{K_1} + T_b - T_{P,0} \right] \right\}, \tag{10}$$

$$B_{1,2} = \left\{ 1 + \frac{K_1}{K_2} - \frac{C_P}{K_2 \tau_{1,2}} \right\} A_{1,2}. \tag{11}$$

The aim of the present setup is to maintain the increase of sample and platform temperature by ΔT. To achieve this, the heat losses have to be compensated by an additional background heating P_h. A constant ΔT implies that $T_P(t)$ and $T_S(t)$ are independent of τ_1 since the heat losses occur through the weak link (described by K_1 and τ_1). This requires that $A_1 = 0$ in Eq. (7). Using this boundary condition in Eq. (10) and defining

$$\Delta T = T_P(t \gg t_2) - T_P(t_1), \tag{12}$$

the temperature of the platform and sample has increased by

$$\Delta T = \frac{\Delta P}{K_1}(1 - e^{-\Delta t_h/\tau_1}), \tag{13}$$

where $\Delta P := P_h - P_b$ is the effectively added power to the platform. For a weak thermal link between platform and temperature reservoir, the condition $\tau_1 \gg \Delta t_h$ is fulfilled and Eq. (13) simplifies to

$$\frac{\Delta P}{\Delta T} \Delta t_h = K_1 \tau_1. \tag{14}$$

The right-hand side of Eq. (14) follows from Eqs. (7)–(9) for $t=0$ and can be written as

$$K_1 \tau_1 \approx (C_S + C_P) \left(1 + \frac{K_1}{K_2} \frac{C_S}{C_S + C_P} \right). \tag{15}$$

In the limit $K_1/K_2 \ll 1$ the total heat capacity $C = C_S + C_P$ of the sample/platform assembly according to Eq. (15) is then determined by the measured quantities of Eq. (14). In the present setup $K_1/K_2 \ll 1$ is fulfilled over a wide temperature range. An exact number, however, is difficult to state since K_2 strongly depends on the shape and the internal thermal conductivity of the sample. Further details about the determination of the heat capacity, the adjustment of the background heating, and the calculation of the heat pulses for a measuring cycle are given in the Appendix.

III. EXPERIMENT DETAILS

A sketch of the sample platform is shown in Fig. 2. The platform is a thin silver plate ($4 \times 3 \times 0.4$ mm^3), with a RuO_2-chip temperature sensor ($m = 0.8$ mg, $R_0 \approx 2k\Omega$ at room temperature) and a resistive heater (10 kΩ film resis-

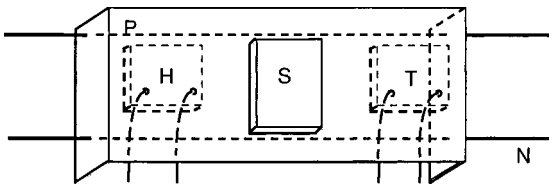

FIG. 2. Schematic view of the platform. *P*, silver platform; *N*, nylon threacd; *S*, sample; *T*, RuO_2-chip temperature sensor; *H*, heater.

tor, $m=2.4$ mg). To realize a low thermal conduction between sample platform and environment the platform is mounted with two thin nylon threads ($\phi=80$ μm) on a silver ring ($\phi=25$ mm). Furthermore, manganin leads ($\phi=30$ μm, length ≈ 10 cm) are used to connect the heater and thermometer to a plug placed on the ring. For this configuration the thermal conductance K_1 varies between 1×10^{-9} W/K at 0.1 K and 1×10^{-7} W/K at 4.2 K. The minimum temperature is limited by K_1 and the residual thermal leak. It comprises the heat input caused by mechanical vibrations of the cryostat, but other sources for energy dissipation, like high frequency noise cannot be ruled out. The residual power is much less than 10 pW and limits the platform temperature to about 30 mK. An additional heat input of the same order of magnitude is produced at the highest magnetic fields and prevents the platform temperature to be less than ≈ 50 mK.

The RuO_2-chip temperature sensor was calibrated in the temperature range 15 mK$<T<$200 mK against a fixed point device (SRM 768 of the former National Bureau of Standards, USA) and against a commercially calibrated RuO_2 thermometer[12] in the temperature range 50 mK$<T<$6 K. The resistance values of the RuO_2-chip sensor, R, were converted to temperature using $\log T=\Sigma_{n=0}^{4} a_n[\log(R-R_0)]^n$, with the fitting parameters a_n. Any strong deviation from a straight line in a $\log(T)$ vs $\log(R-R_0)$ plot immediately reveals self-heating of the sensor during calibration.[13] Temperature sweeps were performed in various (constant) magnetic fields to obtain a sensor calibration at these particular fields. The RuO_2 chip was fixed on the platform (which was thermally anchored to the silver ring) while a calibrated thermometer[12] mounted in the field compensated region of the cryostat was used as a reference. For each field, a $T(R)$ function as given above was used to describe the data. The entire set of $T(R,B)$ data can be used to calculate a calibration for any field value needed during the experiment. In this procedure, particular attention was payed to magnetic field effects on R. The resistance of the RuO_2 sensor is $R\approx 30$ kΩ at 30 mK and its sensitivity, i.e., $\partial \ln R/\partial \ln T$, increases almost linearly from -0.4 at 0.9 K to -0.54 at 30 mK. At the lowest temperatures such an order of magnitude of R is well suited for an ac bridge technique.

In order to determine the addenda of the platform, i.e., the specific heat of the heater, thermometer, wires and grease (Apiezon N), the heat capacity of silver ($m=92.6$ mg, purity: 99.99+%) was measured in zero field and several fields up to 10 T. The addenda in zero field is less than 0.2 μJ/K at 0.1 K and below 0.4 μJ/K at 1 K. No influence of the magnetic field on the addenda could be resolved.

The experimental setup for the calorimetric measurements consists of a dilution refrigerator ($T_{\min}\simeq 15$ mK) with a superconducting magnet ($B_{\max}\simeq 12$ T). Standard digital dc sources and multimeters were used to supply the heating current and to read the voltage drop across the heater. An ac resistance bridge measures the resistance of the RuO_2-chip sensor. As soon as the starting parameters are entered the necessary values like heat-pulse and background-heating current are calculated (see Appendix). Typical values for the applied power are above 10 nW in order to achieve a temperature increase $\Delta T/T_0$ of up to 3%. The duration of the heat pulses are less than 10 s and one measuring cycle can last up to 1000 s. Effects related to τ_2, i.e., a weak coupling of the sample to the platform or a low thermal conductivity of the sample can be detected during the experiment. Then the sample temperature has a characteristic time dependence as depicted in Fig. 1(b). A careful examination of the data clarifies whether the so-called τ_2 effect is negligible or the criterion $K_1/K_2\ll 1$ is violated. In the latter case, the correction term in Eq. (15) has to explicitly taken into account. Since the determination of K_2 is not straightforward, the concerned data are discarded.

IV. APPLICATIONS

A. Tin

A first test of the setup was done with the measurement of the heat capacity of tin. A tin sample ($m=165$ mg, purity: 99.999%) was attached with Apiezon N to the platform and data were recorded from 0.5 K to 6 K. The coefficient of the phonon contribution, βT^3, to the heat capacity is calculated to $\beta=0.28(1)$ mJ mol^{-1} K^{-4}. The heat capacity in the superconducting phase ($T_c=3.72$ K) can be described by $C_{\rm sc}=a\gamma T_c \exp(-bT_c/T)$ with $a=6.0(1)$, $b=1.8(1)$, and $\gamma=1.94(1)$ mJ mol^{-1} K^{-2}. These values are in good agreement with literature data.[14]

This test measurement revealed one drawback related to the weak thermal coupling. The mounting of the platform with the thin nylon threads is not suited for samples with masses larger than ≈ 50 mg. In this case the platform captures vibrations of the cryostat and the performance of the technique is considerably limited for $T<0.3$ K. A better mounting, i.e., thicker threads or even a rigid connection of the platform to the silver ring increase the thermal link. Then, the background heating is not able to compensate the heat losses at high temperature and the method can be used only in a small temperature range. If the sample has an adequate mass and $K_1/K_2\ll 1$ is fulfilled, then a minimum heat capacity of about 1 μJ/K at 0.1 K can be measured.

B. $YbRh_2(Si_{0.95}Ge_{0.05})_2$

In order to test the performance of the compensated heat-pulse method in high magnetic fields the system $YbRh_2(Si_{0.95}Ge_{0.05})_2$ was chosen. $YbRh_2(Si_{0.95}Ge_{0.05})_2$ is a strongly correlated electron system which orders antiferromagnetically at $T_N=20$ mK.[15] This low ordering temperature indicates that the material is very close to a magnetic/nonmagnetic phase transition. The application of an external magnetic field tunes $YbRh_2(Si_{0.95}Ge_{0.05})_2$ through a quantum critical point into a Landau–Fermi liquid state at high field.[15] The heat capacity was carefully measured with a

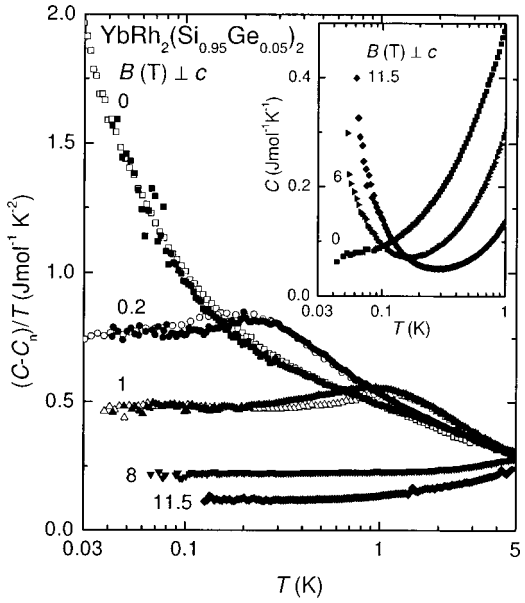

FIG. 3. Temperature dependence of the specific heat divided by temperature $(C-C_n)/T$, of $YbRh_2(Si_{0.95}Ge_{0.05})_2$ in various magnetic fields B applied perpendicular to the crystallographic c axis. The nuclear contributions to the specific heat, C_n, has been subtracted from the raw data. Filled and open symbols represent data obtained with the compensated heat-pulse and relaxation (Ref. 15) method, respectively. Inset, low temperature part of the raw data, C vs T. The strong upturn at low temperature is due to the nuclear-Zeeman contribution to the total specific heat.

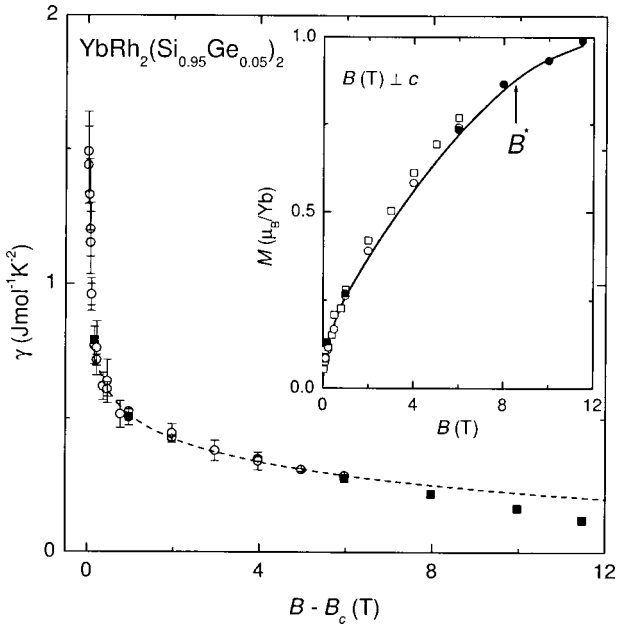

FIG. 4. Magnetic field dependence of $\gamma=(C-C_n)/T$ for $T\to 0$ of $YbRh_2(Si_{0.95}Ge_{0.05})_2$. $B_c=0.027$ T is a critical field. Data depicted as open symbols are taken from Ref. 15. Inset, field dependence of calculated [open symbols (Ref. 15)] and measured magnetization [solid-line (Ref. 15)] at 40 mK. The slope of $M(B)$ changes at $B^*\approx 8.5$ T.

relaxation technique in magnetic fields up to 6 T (Ref. 15) while the present setup allowed the field range to be extended up to 11.5 T. Furthermore, the absolute value of the heat capacity can be directly compared with the data reported in Ref. 15 since they were obtained on the *same* sample ($m=21$ mg).

Figure 3 shows a comparison of the specific heat capacity $(C-C_n)/T$ vs temperature of $YbRh_2(Si_{0.95}Ge_{0.05})_2$ obtained with the two techniques. Here, C_n denotes the nuclear contributions to the specific heat (see below). The zero field values below 0.1 K and above 0.2 K agree within 2%, between 0.1 K and 0.2 K the deviation is less than 5%. The slight deviations close to a maximum at $T_0(B)$ at 0.2 K ($B=0.2$ T) and at 1 K ($B=1$ T) are not related to the measuring technique. It presumably results from a small difference in the applied magnetic fields since the maximum is very sensitive to an external magnetic field. This comparison corroborates that the compensated heat-pulse method can be used to measure the heat capacity in a wide temperature range in magnetic fields up to 12 T.

Several raw data sets, $C(T)$, are depicted in the inset to Fig. 3. The nuclear contributions C_Q and $C_{\rm hf}$ to the heat capacity lead to an increase of $C(T)$ at low temperatures. The field-independent quadrupolar contribution $C_Q=\alpha_Q/T^2$ has to be subtracted from the raw data below about 0.1 K. α_Q/T^2 represents the high-temperature part of the nuclear-Schottky anomaly and α_Q was estimated to $\alpha_Q=5.68\times 10^{-6}$ J K mol^{-1} by Mössbauer experiments on the electrical quadrupole splitting [16] of the nuclear spin $I=5/2$ of ^{173}Yb (natural abundandance of 0.162). The field-induced part to the heat capacity, i.e., the nuclear-Zeeman contribution $C_{\rm hf}=\alpha(B)/T^2$, was deduced from plotting CT^2 vs T^3. This yields $\alpha(B)$ and the Sommerfeld coefficient $\gamma(B)$. The latter value is plotted in Fig. 4 together with the data of Ref. 15 vs $B-B_c$. Here, $B_c=0.027$ T is a critical field, deduced from the occurrence of a shallow maximum in $(C-C_n)/T$ at a characteristic temperature $T_0(B)$. The latter depends linearly on the field.[15] The reliability of the graphical determination of $\alpha(B)$ can be checked by calculating the field dependence of the magnetization, $M(B)$. It can be calculated via $(B_{\rm hf}-B)/A_{\rm Yb}$, with $A_{\rm Yb}$ the hyperfine coupling constant and the hyperfine field $B_{\rm hf}=\sqrt{(\alpha(B)-\alpha_Q)/\alpha_{\rm dip}}$. The gyromagnetic ratio $\alpha_{\rm dip}=0.076\times 10^{-6}$ J K mol^{-1} T^{-2} is known from nuclear magnetic resonance data.[17] The magnetization estimated from the heat capacity can be matched to the measured $M(B)$ curve if $A_{\rm Yb}=20\ {\rm T}/\mu_B$ is assumed (see inset to Fig. 4). This value is of the same order as the value found in Yb_4As_3.[18]

The diverging γ value on approaching small magnetic fields was one strong argument for the conclusion in Ref. 15 that the most critical scattering is local. In the present context, however, the $\gamma(B)$ dependence at high fields is of interest. The data reported in Ref. 15 (open symbols in Fig. 4) above $B-B_c=0.3$ T were described by $\gamma=a\ \ln[b/(B-B_c)]$, with $a=0.126(4)$ J mol^{-1} K^{-2} and $b=59(7)$ T, as predicted in a two-dimensional (2D) spin-density-wave scenario (dashed line in Fig. 4). The data from the present experiment show a deviation from such a field dependence above ≈ 8 T. At a field value $B^*\approx 8.5$ T the $M(B)$ curve (solid line in inset to Fig. 4) starts to change slope. A similar anomaly in $M(B)$ of $YbRh_2Si_2$ (Ref. 19) has been interpreted as a signature of the complete localization of the $4f$ electrons. In this case the renormalization of the heavy-electron density of states, measured by γ, should be reduced above B^*. This is seen in Fig. 4, where the 2D spin-density-wave scenario is extrapolated to high fields. The deviation of $\gamma(B)$ from this extrapolation shows that the $4f$ electrons are completely localized and the

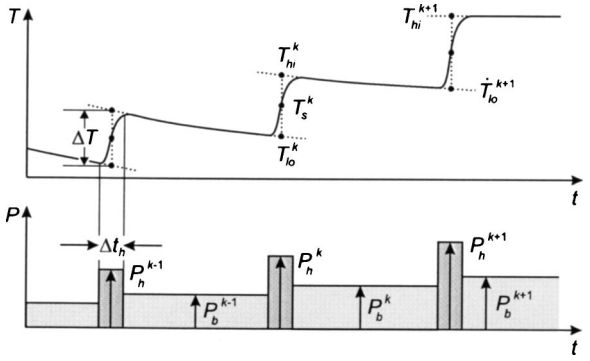

FIG. 5. Time dependence of the sample temperature T_S, the power of the heat pulse P_h, and the background heating P_b for several measuring cycles. In cycle k a heat pulse supplies the electrical power P_h^k to the platform. It increases the sample temperature by $\Delta T = T_{\rm hi}^k - T_{\rm lo}^k$. The determination of the heat capacity C^k at T_S^k takes the temperature drifts $\dot{T}_{\rm lo}^{k+1}$ and $\dot{T}_{\rm hi}^{k+1}$ into account (see text). The background heating P_b^k is adjusted for each cycle.

heavy-fermion state is suppressed at magnetic fields above B^*, like in $YbRh_2Si_2$.[19]

ACKNOWLEDGMENTS

We are deeply grateful to N. E. Phillips and R. A. Fisher for introducing R. Caspary into the semiadiabatic heat-pulse technique during its development. It is a pleasure to thank K. Neumaier at the Walther Meissner Institute for Low Temperature Research of the Bavarian Academy of Science in Garching for many fruitful discussions and U. Ließ for technical support. We thank O. Trovarelli for supplying the high quality single crystal of $YbRh_2(Si_{0.95}Ge_{0.05})_2$ and Y. Tokiwa for providing the magnetization data. P. Gegenwart is acknowledged for discussions about $YbRh_2Si_2$ in high magnetic fields.

APPENDIX: MEASURING PROCEDURE

The computer-controlled measuring routine performs for each cycle k the determination of the heat capacity C^k, the adjustment of the background heating P_b^{k+1}, and the estimation of the new heat-pulse power P_h^{k+1}. In order to clarify the procedure, the time variation of the sample temperature and the supplied power to the platform is sketched in Fig. 5. In the course of time the background heating as well as the power of the heat pulse increase to compensate the temperature dependent heat leak and to achieve the desired increase of the sample's temperature, respectively. The heat capacity of the sample, $C(T_S^k)$, during the measuring cycle k at the mean sample temperature

$$T_S^k = \tfrac{1}{2}(T_{\rm lo}^k + T_{\rm hi}^k) \tag{A1}$$

is given by

$$C^k := C(T_S^k) \simeq P\frac{\Delta t}{\Delta T} = (P_{\rm in}^k - P_{\rm out}^k)\frac{\Delta t_h}{T_{\rm hi}^k - T_{\rm lo}^k}. \tag{A2}$$

The incoming power $P_{\rm in}^k$ is equal to P_h^k whereas the heat flow $P_{\rm out}^k$ to the temperature bath is taken as the average of the out flowing heat $P_{\rm out,lo}^k$ immediately before the heat pulse

$$P_{\rm out,lo}^k = P_b^{k-1} - C_{\rm lo}^k \dot{T}_{\rm lo}^k \tag{A3}$$

and immediately after the heat pulse

$$P_{\rm out,hi}^k = P_b^k - C_{\rm hi}^k \dot{T}_{\rm hi}^k. \tag{A4}$$

Here, $\dot{T}_{\rm hi}^k$ and $\dot{T}_{\rm lo}^k$ are the temperature drifts at $T_{\rm hi}^k$ and $T_{\rm lo}^k$, respectively (see Fig. 5).

In order to eliminate $C_{\rm lo}^k$ and $C_{\rm hi}^k$ in Eqs. (A3) and (A4), respectively, a linear temperature dependence of C^k is assumed. Then, using Eq. (A2) the heat capacity C^k is determined by

$$C^k \approx \frac{2P_h^k - (P_b^{k-1} + P_b^k) + [(1 - f_{\rm lo}^k)\dot{T}_{\rm lo}^k + (1 - f_{\rm hi}^k)\dot{T}_{\rm hi}^k]C^{k-1}}{2(T_{\rm hi}^k - T_{\rm lo}^k)/\Delta t_h - (f_{\rm lo}^k \dot{T}_{\rm lo}^k + f_{\rm hi}^k \dot{T}_{\rm hi}^k)} \tag{A5}$$

with the coefficients $f_{\rm lo}^k$ and $f_{\rm hi}^k$ defined as

$$f_{\rm lo}^k = \frac{T_{\rm lo}^k - T_S^{k-1}}{T_S^k - T_S^{k-1}}$$

and

$$f_{\rm hi}^k = \frac{T_{\rm hi}^k - T_S^{k-1}}{T_S^k - T_S^{k-1}}.$$

Due to the temperature dependence of the thermal conductances K_1 and K_2 the heat losses increase with increasing temperature. This requires to adjust the background heating after each heat pulse. Such an adjustment will never be ideal and results in a temperature drift $\dot{T}_{\rm hi}^k \neq 0$ during the measuring cycle k. Thus, the chosen background heating P_b^k must be corrected by

$$P_{\rm corr}^k = -C_{\rm hi}^k \dot{T}_{\rm hi}^k \approx -[f_{\rm hi}^k C^k + (1 - f_{\rm hi}^k)C^{k-1}]\dot{T}_{\rm hi}^k. \tag{A6}$$

This can be extrapolated to obtain an optimized background heating for the next step,

$$P_b^{k+1} \approx P_b^{k-1} + P_{\rm corr}^{k-1} + \frac{T_{\rm hi}^{k+1} - T_{\rm hi}^{k-1}}{T_{\rm hi}^k - T_{\rm hi}^{k-1}} \times [(P_b^k + P_{\rm corr}^k) - (P_b^{k-1} + P_{\rm corr}^{k-1})]. \tag{A7}$$

The heat capacity of the sample in the next cycle might be different and therefore, the power of the heat pulse has to be re-estimated. It has to ensure that the desired temperature increase $\Delta T = T_{\rm hi}^{k+1} - T_{\rm lo}^{k+1}$ is achieved. Thus, the power for the new heat pulse is according to Eq. (A2) approximated by

$$P_h^{k+1} = P_{\rm in}^{k+1} \approx C^{k+1}\frac{T_{\rm hi}^{k+1} - T_{\rm lo}^{k+1}}{\Delta t_h} + P_{\rm out}^{k+1}. \tag{A8}$$

This approximation depends on an estimate of the expected heat capacity and heat loss in the following measuring cycle. An estimation of C^{k+1} can be obtained by a linear extrapolation of the two preceding heat capacities:

$$C^{k+1} \approx f_S^{k+1} C^k + (1 - f_S^{k+1})C^{k-1}. \tag{A9}$$

The heat flow $P_{\rm out}^{k+1}$ to the bath is according to Eq. (A7), with the requirement $\dot{T}_{\rm hi}^{k+1} \equiv 0$, given by

$$P_{\rm out}^{k+1} \approx (P_b^{k+1} + P_b^k)/2 - [g_{\rm lo}^{k+1} C^k + (1 - g_{\rm lo}^{k+1})C^{k-1}]\dot{T}_{\rm lo}^{k+1}/2, \tag{A10}$$

using the coefficient

$$g_{\mathrm{lo}}^{k+1} = \frac{T_{\mathrm{lo}}^{k+1} - T_S^{k-1}}{T_S^k - T_S^{k-1}}.$$

With Eqs. (A9) and (A10) the new heat pulse P_h^{k+1} eventually results to

$$P_h^{k+1} \approx (P_b^{k+1} + P_b^k)/2 + \left[f_S^{k+1} \frac{T_{\mathrm{hi}}^{k+1} - T_{\mathrm{lo}}^{k+1}}{\Delta t_h} - \frac{g_{\mathrm{lo}}^{k+1}}{2} \dot{T}_{\mathrm{lo}}^{k+1} \right] C^k + \left[(1 - f_S^{k+1}) \frac{T_{\mathrm{hi}}^{k+1} - T_{\mathrm{lo}}^{k+1}}{\Delta t_h} - \frac{1 - g_{\mathrm{lo}}^{k+1}}{2} \dot{T}_{\mathrm{lo}}^{k+1} \right] C^{k-1}, \tag{A11}$$

using the definition

$$f_S^{k+1} = \frac{T_S^{k+1} - T_S^{k-1}}{T_S^k - T_S^{k-1}}.$$

The computer controlled routine needs as input parameter the desired temperature increase ΔT and the temperature range. The measurement runs automatically as long as no sharp feature in $C(T)$ occurs. Even in the case of a first order phase transition the extrapolations in Eqs. (A9)–(A11) yield a good estimate and the computer-controlled sequence runs without problems.

[1] R. Bachmann, F. J. Disalvo Jr., T. H. Geballe, R.-L. Greene, R. E. Howard, C. N. King, H. C. Kirsch, K. N. Lee, R. E. Schwall, H.-U. Thomas, and R. B. Zubeck, Rev. Sci. Instrum. **43**, 205 (1972).

[2] J. F. Cochran, C. A. Shiffman, and J. E. Neighbor, Rev. Sci. Instrum. **37**, 499 (1966).

[3] P. F. Sullivan and G. Seidel, Phys. Rev. **173**, 679 (1968).

[4] R. E. Schwall, R. E. Howard, and G. R. Stewart, Rev. Sci. Instrum. **46**, 1054 (1975).

[5] E. Gmelin, Thermochim. Acta **29**, 1 (1979).

[6] G. R. Stewart, Rev. Sci. Instrum. **54**, 1 (1983).

[7] Y. Kraftmakher, Phys. Rep. **356**, 1 (2002).

[8] R. A. Fisher, P. Radhakrishna, N. E. Phillips, J. V. Badding, and A. M. Stacy, Phys. Rev. B **52**, 13519 (1995).

[9] R. Caspary, Ph.D thesis, Technische Hochschule Darmstadt, 1993.

[10] P. Hellmann, Diploma thesis, Technische Hochschule Darmstadt, 1993.

[11] $T_P(t)$ in Fig. 1(b) was calculated using the following quantities: $T_0 = 70$ mK, $C_S = C_P = 1$ μJ/K, $K_2 = 100$ nW/K, $K_2/K_1 = 100$, $\Delta t_h = 7$ s, $\Delta T/T_0 = 3\%$, $P_h = 0.7$ nW, $P_b = 42$ pW.

[12] The RuO_2 thermometer, RX-102-AA-M, was calibrated by the manufacturer, Lake Shore Cryotronics, Inc., using the ITS-90 temperature scale.

[13] The temperature dependence of the resistance of the RuO_2-chip sensor has been analyzed in terms of a charge transport due to variable-range hopping between localized states close to the Fermi level. The data can be described by $R(T) \propto \exp[(T_0/T)^\alpha]$ with $\alpha = 0.47$ and $\alpha = 0.21$ for $T > 1$ K and $0.2\ \mathrm{K} < T < 2\mathrm{K}$, respectively. Nevertheless, the polynomial calibration function was used since it is a continuous and smooth function.

[14] H. R. O'Neal and N. E. Phillips, Phys. Rev. **137**, A748 (1965).

[15] J. Custers, P. Gegenwart, H. Wilhelm, K. Neumaier, Y. Tokiwa, O. Trovarelli, C. Geibel, F. Steglich, C. Pépin, and P. Coleman, Nature (London) **425**, 525 (2003); cond-mat/0308001.

[16] J. Plessel, Ph.D. thesis, University Cologne, 2001.

[17] G. C. Carter, L. H. Bennett, and D. J. Kahan, *Metallic shifts in NMR, Progress in Materials Science* (Pergamon, Oxford, 1977), Vol. 20, Chap. 9, p. 123.

[18] P. Bonville, A. Ochiai, T. Suzuki, and E. Vincent, J. Phys. I **4**, 595 (1994).

[19] Y. Tokiwa, P. Gegenwart, F. Weickert, R. Küchler, J. Custers, J. Ferstl, C. Geibel, and F. Steglich, J. Magn. Magn. Mater. **272–276**, e87 (2004).